Strain Analysis and Engineering in Halide Perovskite Photovoltaics

Dongtao Liu[1,5], *Deying Luo*[2,5], *Affan N. Iqbal*[3,4,5], *Kieran W. P. Orr*[3,4,5], *Tiarnan A. S. Doherty*[3], *Zheng-Hong Lu*[2], *Samuel D. Stranks*[3,4†], *Wei Zhang*[1†]

[1]Advanced Technology Institute, University of Surrey, Guildford GU2 7XH, United Kingdom.

[2]Department of Materials Science and Engineering, University of Toronto, Toronto M5G 3E4, Canada.

[3]Cavendish Laboratory, Department of Physics, University of Cambridge, J.J. Thomson Avenue, Cambridge CB3 0HE, United Kingdom.

[4]Department of Chemical Engineering & Biotechnology, University of Cambridge, Philippa Fawcett Drive, Cambridge CB3 0AS, United Kingdom.

[5]These authors contributed equally to this work.

[†]Corresponding author: E-mail: wz0003@surrey.ac.uk (W.Z.), sds65@cam.ac.uk (S.D.S).

Abstract

Halide perovskites are a compelling candidate for the next generation of clean energy harvesting technologies thanks to their low cost, facile fabrication and outstanding semiconductor properties. However, photovoltaic device efficiencies are still below practical limits and long-term stability challenges hinder their practical application. Current evidence suggests that strain in halide perovskites is a key factor in dictating device efficiency and stability. Here, we outline the fundamentals of strain within halide perovskites relevant to photovoltaic applications and rationalize approaches to characterize the phenomenon. We examine recent breakthroughs in eliminating the adverse impacts of strain, enhancing both device efficiencies and operational stabilities. Finally, we discuss further challenges and outline future research directions for placing stress and strain studies at the forefront of halide perovskite research. An extensive understanding of strain in halide perovskite is needed, which would allow effective strain management and drive further enhancements in efficiencies and stabilities of perovskite photovoltaics.

Halide perovskites have been thrust into the limelight in the last decade as a promising next-generation photovoltaic technology, with power conversion efficiencies (PCEs) already comparable with those of crystalline silicon devices. Reductions in unwanted energy losses both in the absorber and at interfaces with contact layers have led to substantial efficiency and stability improvements. Recently, strain control has been at the forefront of device efficiency enhancement in halide perovskites by minimizing undesirable defect formation[1,2], and subsequent nonradiative recombination[3]. A certified PCE of ~24.4% has recently been reported for $FAPbI_3$-based devices (FA=formamidinium) through managing strain, with the encapsulated devices retaining 90% of their efficiencies after 400 hours at maximum power point[1]. Such encouraging achievements suggest that strain engineering is a powerful tool to enhance efficiencies and stabilities for a broad range of practical applications. Despite such successes, there is an apparent paradox whereby similarly strained halide perovskites exhibit either beneficial or detrimental effects even when they are nominally similar materials. Furthermore, the magnitude of strain is relatively high in halide perovskites compared to other photovoltaic systems: for instance, residual strain values of up to ~2.4% for α-$FAPbI_3$[4] and ~1.6% for $CsPbBr_3$ have been reported[5], whereas the performance of Si and Cu(In, Ga)Se_2 devices drops substantially when residual strains exceed ~1%[6,7]. The high magnitude of strain in perovskite materials is particularly striking since perovskites are one of the most mechanically fragile of any photovoltaic materials[8]. It is therefore essential to thoroughly understand the fundamentals of strain on different length scales, and to devise effective methods to characterise it. This will allow us to move towards rational engineering as opposed to empirical optimisation.

1. Definition and measurement of strain in halide perovskites

Strain (ε) is defined as a structural deformation of a material in response to applied stress(σ)[9]. This stress can be from external forces on the material, or internal structural defects such as atomic interstitials and vacancies. Mathematically, strain is defined by a (second rank) tensor with elements given by

$$\epsilon_{kl} = \frac{1}{2}(e_{kl} + e_{lk}) \, .$$

Here, $e_{kl} = \frac{\partial u_k}{\partial x_l}$, where u_k are the components of the atomic displacement vector $\mathbf{u}(x_1, x_2, x_3)$ along the Cartesian directions, and x_l are the Cartesian coordinates. $\mathbf{u}(x_1, x_2, x_3)$ describes the displacement of atoms from their expected positions in an unstrained material, and the above definition is valid for small displacements. This particular linear combination of $\frac{1}{2}(e_{kl} + e_{lk})$ removes the effects of rigid rotation from the strain tensor[10]. Determination of this tensor constitutes a full description of strain in materials as the atomic displacement vectors can be reconstructed from the tensor elements. Such a description not only encapsulates the length changes along the Cartesian axes given by $\varepsilon_{x_1x_1}$, $\varepsilon_{x_2x_2}$, and $\varepsilon_{x_3x_3}$, but also the shear components of the deformation given by the off-diagonal elements. In the elastic regime, the magnitude of the deformation resulting from the applied stress (also a tensor, σ) can be

calculated from Hooke's law, $\sigma_{ij} = c_{ijkl}\varepsilon_{kl}$, where c_{ijkl} are the components of a (fourth rank) stiffness tensor.

The aspects of strain in a material that can be determined with typical laboratory techniques include tensile and compressive strain where the interplanar spacing, d, of the material is compared to a reference "unstrained" value. Typically, the variation in d spacing is observed through the Bragg peak positions in an X-ray diffraction (XRD) pattern. If a material is compressively strained, the d spacing is decreased relative to the reference, and the peak associated with that plane will shift to higher scattering vector, $\mathbf{q}$ (Fig. 1a,b), with the converse being true for tensile strain. The values of compressive/tensile strain are usually expressed as a ratio of the d spacings and written as percentages. The nature of strain (compressive/tensile) is indicated either explicitly or using a negative/positive sign indicating compressive/tensile strain, respectively. However, we note that such measurements only probe the diagonal (ε_{kk}) elements of the strain tensor. Furthermore, applying a load (stress) to a material results in deformations (strain) not only in the directions parallel to, but also perpendicular to the load (Poisson's effect). For example, a biaxial in-plane tensile strain in a halide perovskite thin film will also result in a compressive strain in the direction of the film normal[11]. This is especially pertinent because many lab-based X-ray diffractometers are in Bragg-Brentano (reflection) geometry with the scattering vector in the direction of the film normal. Consequently, it is the out-of-plane compressive strain that will be probed.

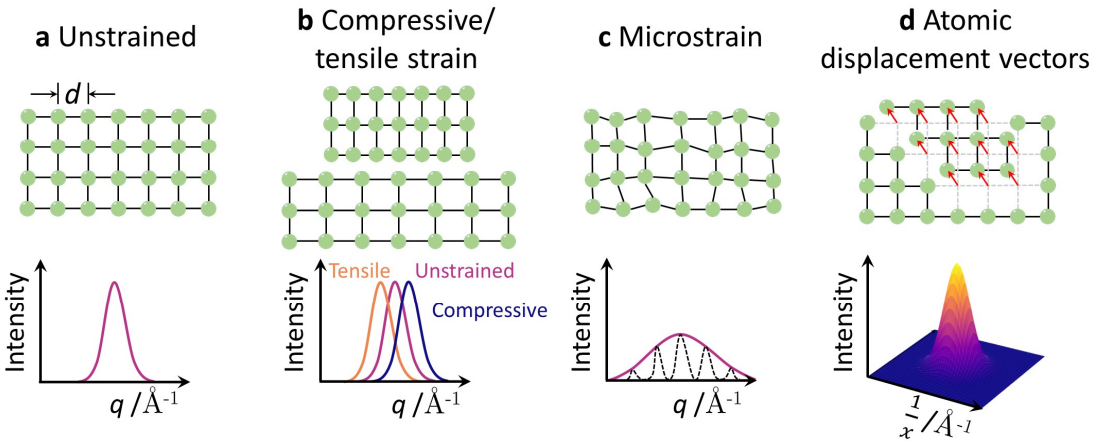

Fig. 1| Definition and measurement of strain in halide perovskites. a-d, The top row gives representations of (**a**) unstrained material, (**b**) compressive/tensile strain, (**c**) microstrain, and (**d**) atomic displacement vectors. The bottom row indicates the signatures of each of these kinds of strain in diffraction patterns.

An additional feature of strain reported is "microstrain" which is determined by Bragg peak width analyses. If the diffraction measurement simultaneously samples a number of different d spacings within the sample, then contributions from all these d spacings will combine to form a broadened Bragg peak (Fig. 1c). Microstrain is a measure of local deviations of d spacings from their average value and includes contributions from both locally compressively and locally tensile strained regions. A commonly employed method for calculating microstrain

is Williamson-Hall analysis[12]. The method relies on the different q-dependence of Bragg peak broadening resulting from microstrain and crystallite size effects and, despite the method's ubiquity, there are many potential pitfalls. One must first remove any instrument broadening, which is typically accomplished using an external standard, but these standards may not be in the same form as the sample (e.g. thin film) and thus do not exactly reproduce the conditions of the diffractometer for the sample. Further, many nuances influence the crystallite size calculation including the distribution of sizes, shape, and crystallite length in each crystallographic direction. Errors in calculation of particle size will have a knock-on effect for determination of microstrain. Depending on the structural features (dislocations, variable lattice distortion, grain surface relaxation) there may or may not be a strong hkl dependence on microstrain peak broadening, which complicates matters further. Therefore, the researcher must be especially diligent when carrying out peak broadening analyses from lab-based bulk XRD measurements[12]. We also stress that microstrain values are not directly comparable to compressive/tensile strain values given that these two quantities probe different aspects of material structure. The community must avoid interchangeable use of these terminologies to prevent errors.

Another important consideration is the relevant length scale of the measurement. All of the lattice planes that satisfy the Bragg condition within the sample interaction volume (defined by the footprint and penetration depth) of the X-rays contribute to a given diffraction peak. In most lab-based X-ray diffractometers, the beam footprint is on the scale of millimetres squared and so the interaction volume is large and variations in d spacings in this region result in a broadened Bragg peak. However, by reducing the beam footprint and scanning the illumination position across the sample, the local shifts in d spacing can be resolved in the form of a tensile and compressive strain map. This forms the basis for spatially resolved XRD techniques (micro- or nano-XRD) that are able to measure local peak shifts or phase changes[3]. Overall, one must consider the relevant length scales to probe in halide perovskites given that heterogeneities are present over nanometers up to many micrometers[13].

Other advanced techniques are required to probe beyond the diagonal elements of the strain tensor corresponding to structure expansion/contraction. By using the three-dimensional intensity distribution around Bragg peaks, one can reconstruct the electron density of a crystal to find the atomic displacement vectors (Fig. 1d) from which the off-diagonal components of the strain tensor can be extracted. Techniques that can provide such rich information even on the local scale include Bragg coherent diffraction imaging and Bragg ptychographic approaches[14, 15].

2. Origins of strain in halide perovskites

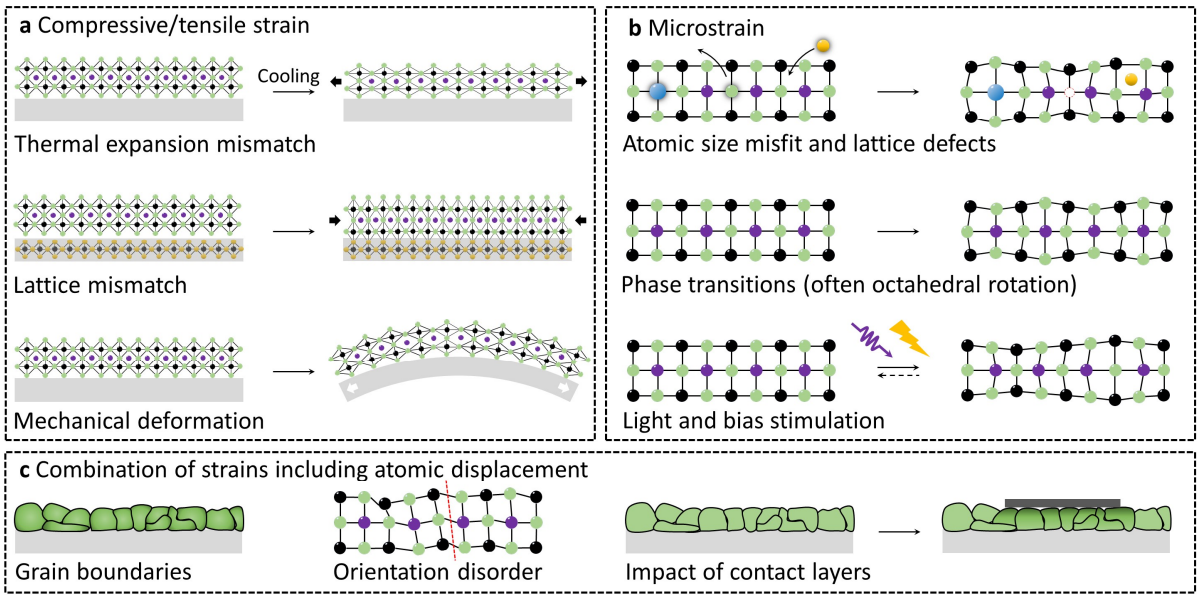

Fig. 2| Origins of strain in halide perovskites. a-c, Representations of the origins of (**a**) compressive/tensile strain, (**b**) microstrain, and (**c**) more complex strain (including contributions from shear and rotational components of the strain tensor) in halide perovskites. The blue and purple spheres are the A-site cations (e.g., Cs, MA and FA), and the black and green spheres represent metal cations (e.g., Pb, Sn) and halide anions (e.g., Cl, Br and I), respectively. In **a**, the orange spheres are substrate atoms. In (**b**), the red dashed circle is a vacancy, and the yellow sphere represents the extrinsic dopant that causes a defect. The red dashed line in (**c**) indicates a twin boundary.

Strain can result from a broad range of factors. During film formation, the precursor solutions are deposited on a substrate and the film is annealed (often above 100 °C). If the film is formed on a substrate with a lower coefficient of thermal expansion (CTE) than the perovskite (3.3~8.4 $\times 10^{-5}$ K^{-1})[16], the substrate restricts the contraction of the perovskite along the in-plane directions during cool down[17], resulting in an in-plane tensile strain (Fig. 2a, top). Analogously, compressive strain can occur in a film grown on a substrate with a higher CTE than that of the perovskite, though this is less common in halide perovskite devices. This process of cooling after annealing leads to strain (generally tensile) in the plane of the film.

Lattice mismatch between the substrate and the as-formed perovskite film can also generate a tensile or compressive strain (Fig. 2a, middle), depending on whether the *d* spacing of the substrate is larger or smaller than that of the perovskite overlayer. However, when the lattice mismatch is large, the perovskite crystal randomly stacks on the bottom crystal, resulting in a non-uniform interfacial distortion[18, 19]. Compressive and tensile strains can also be introduced to films using mechanical film bending[20] (Fig. 2a, bottom) and hydrostatic pressure[21].

While the above factors generally influence strains across the whole film, other factors including atomic misfits, phase transitions, light/bias stimulation and grain boundaries are linked to local strain (namely microstrain) in halide perovskites (Fig. 2b). For example, in $FAPbI_3$, the large FA cation within the 3D structure promotes local PbI_6 octahedral tilting (that

is, the Pb-X-Pb angle deviates from the ideal 180°), resulting in a local lattice distortion[2, 22]. Further, local lattice distortion and strain are greatly elevated during phase transitions, where the symmetry of the crystal structure is generally lowered compared to the cubic perovskite structure. Group theoretical analysis[23] of octahedral tilting schemes yields group-subgroup relationships between perovskite phases (e.g. *I4/mcm* is a subgroup of $Pm\bar{3}m$) which can transform in a continuous (i.e., second-order) fashion, leading to spontaneous strains due to continuous lattice parameter variation between phases upon octahedral tilting[24-26]. Large strains and complex microstructure, such as martensitic nano/microstructures[26] or crystal twins, can result from discontinuous (i.e., first-order) phase transitions with abrupt changes in lattice parameter, which can occur between non-group-subgroup related space groups (though first-order transitions between group-subgroup phases are also possible). Such a transition is found in $MAPbI_3$ (MA = methylammonium) between *I4/mcm* to $Im\bar{3}$, at a hydrostatic pressure of ~0.3 GPa[21]. Martensitic transformations are diffusionless and often involve a lowering of crystal symmetry (e.g., from cubic to tetragonal[27]) and when the resulting phases are mutually spatially constrained, strain minimisation can result in a change in shape and curvature of their interface[28]. Therefore, one can use strain to vary the nano/microstructure resulting from martensitic transformations, as has been shown, for example, in $SrSnO_3$[29]. Given the prevalence of symmetry lowering phase transitions in halide perovskites, a more detailed understanding of the strains resulting from phase transitions will be beneficial.

Photovoltaic devices are exposed to light and bias during operation, and these have been reported to affect microstrain in halide perovskites. Recently, it was suggested that microstrain is enhanced under illumination owing to light-assisted ion migration and/or phase segregation[30, 31]. Here, it was proposed that photoexcited carriers within perovskites interact with the soft, ionic lattice[32, 33], resulting in greater microstrain. Further, some works attempt to probe the links between photo-induced lattice expansion and microstrain (excluding the effect of ion migration), but debate is ongoing[34, 35]. Under illumination, the polarity (positive or negative) and magnitude of bias voltages have also been reported to be critical in inducing microstrain by enhancing ion migration[30].

Grain boundaries can be another source of strain in halide perovskites (Fig. 2c, left) with the resulting strain dependent on the specific interfacial conditions, e.g., orientation mismatch at boundaries[36], of which there is striking variation within thin films. It has been proposed that defect formation at certain grain boundaries in perovskite thin films stems from asymmetric strain fields at junctions between grains[37]. The high degree of lattice distortion and non-stoichiometric chemical distribution at grain boundaries also cause large strain fields[3, 38]. Apart from boundaries between grains, sub-grain lattice orientation disorder[36] (Fig. 2c, middle) and twin boundaries may also be sources of strain in halide perovskite films[39]. Contact layers are also known to exert forces on the adjacent perovskite films in devices, however, we note that this is highly dependent on the thickness and stiffness of contact layers (Fig. 2c, right)[20, 40]. Given the substrate's comparatively larger thickness, the substrate will dominate in imparting strain in perovskite devices[20].

3. The effects of strain on halide perovskites

Strain affects the structure of halide perovskites and consequently influences the optoelectronic properties and stability of the material, which both need to be optimised to push perovskite devices towards commercialization.

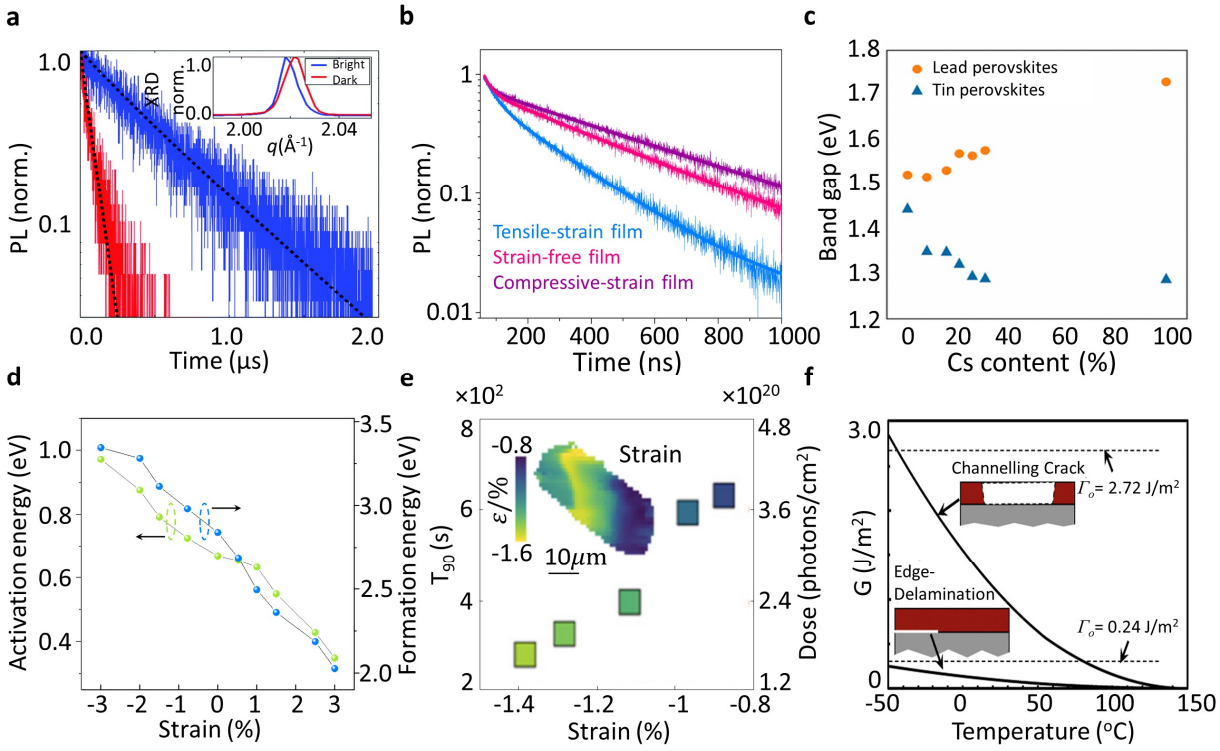

Fig. 3| Effects of strain on halide perovskites. a, Time-resolved photoluminescence (PL) decays for differently strained regions of a $MAPbI_3$ film where the PL lifetime in the more compressively strained region (red; dark PL) is shorter than that in the more tensile strained region (blue; bright PL). Inset: 220 Bragg peaks show the difference in lattice spacing for the two regions. **b**, Time-resolved PL decays for three $(FAPbI_3)_{0.85}(MAPbBr_3)_{0.15}$ films with different strains. **c**, The variation of bandgap with Cs content (scales with lattice parameter) for $FA_{1-x}Cs_xPbI_3$ (orange circles) and $FA_{1-x}Cs_xSnI_3$ (blue triangles). **d**, Calculated strain-dependent activation energies of ion migration and formation energies of halide vacancies in $CsPbI_2Br$ where the minus/plus values in the *x*-axis represent compressive/tensile strain, respectively. **e**, Time for the XRD pattern correlation coefficient to decay to 90 % of its original value (T_{90}) against strain. The right *y*-axis shows the sample's radiation dose. Inset: strain map of the $CsPbBr_3$ microcrystal from which these data are taken. **f**, Calculated strain energy release rate, *G*, for channelling cracks and edge delamination. Γ_0=0.24 J/m^2 (polycrystalline) and Γ_0=2.72 J/m^2 (single-crystalline) are minimum and maximum cohesive fracture energies for $MAPbI_3$, respectively. Figures adapted with permission from: **a**, ref.[3] under a Creative Commons licence (https://creativecommons.org/licenses/by/3.0/); **b**, ref.[41] under a Creative Commons licence (https://creativecommons.org/licenses/by/4.0/); **c**, ref.[43], American Chemical Society; **d**, ref.[16] under a Creative Commons licence (https://creativecommons.org/licenses/by/4.0/); **e**, ref.[5], American Chemical Society; **f**, ref.[11], Elsevier.

3.1 Impact on device performance

The impact of strain on device performance is complicated by the apparently contrasting responses of different perovskite systems to strain and the problem of defining an 'unstrained' reference state. To illustrate this, Fig. 3a shows time-resolved photoluminescence (PL) for a $MAPbI_3$ film[3], showing regions with greater local compressive strain (relative to the average d spacing of the film) associated with the shorter PL lifetime, albeit the net strain on the film is unknown. By contrast, in $(FAPbI_3)_{0.85}(MAPbBr_3)_{0.15}$ films (Fig. 3b) the PL lifetime is reported to increase upon compressive strain[41]. The reason for these apparent differences may be complex, and one must consider how to best benchmark absolute strain and how the different compositions or growth methods will impact both strain and recombination, for example, due to photodoping in the mixed-component systems[42]. Further, Fig. 3c shows that the bandgap increases for $FA_{1-x}Cs_xPbI_3$ but decreases for $FA_{1-x}Cs_xSnI_3$ with increasing Cs content, despite a reduction in lattice parameter in both cases[43]. These conflicting trends are attributed to octahedral tilting dominating over isotropic structural contraction in $FA_{1-x}Cs_xPbI_3$ and highlight the importance of probing the various structural degrees of freedom in the perovskite.

To maximise device efficiency, any nonradiative recombination must be minimised as this leads to power losses. While most defects in halide perovskites are benign, there are still deep trap states, which are detrimental to performance. For example, large variations of intragrain crystallographic orientations and concomitant local strains are linked to higher trap densities[36]. Furthermore, larger grains exhibit more sub-grain misorientation leading to higher trap densities. This suggests that managing local strain is even more critical than tuning morphological grain size for minimising nonradiative recombination. At the sub-grain level, twinning has been shown to be ubiquitous in FA-based systems due to the low twin formation energies[44]; however, these are expected to be benign from a carrier recombination perspective[39].

To understand the effects of strain on the band structure of halide perovskites we must first recognise that the valence band is governed by the anti-bonding overlap between Pb *s* orbitals and halide *p* orbitals, while the conduction band is dominated by the non-bonding overlap between Pb *p* orbitals with minor contributions from halide *p* orbitals. Strain-induced changes in Pb-X bond lengths and bond angles (Pb-X-Pb) and associated changes in orbital overlaps lead to changes in band dispersion[45]. In turn, the bandgap increases with increasing tensile strain and decreases with increasing compressive strain[41]. Carrier mobility has been shown to increase with increasing compressive strain due to a reduction of carrier effective mass, though at higher magnitudes of compressive strain the mobility decreases due to generation of dislocations[4]. In 2D A_2PbBr_4 [(A= *n*-butylammonium, *n*-octylamonium, or phenethylammonium (PEA)][46], mobility was increased by tuning the cation stacking pattern, alleviating microstrain, and reducing electron-phonon interactions. Few-layer 2D perovskites are also observed to exhibit an expanded structure accompanied by a blue-shifted PL emission peak in comparison to bulk 2D perovskites[47]. These reports show that strain is a key optimisation parameter and an essential structural lever for modulating device performance.

3.2 Impact on device stability

Intrinsic device stability is arguably the most important topic for halide perovskites. Ion migration has been associated with device instability, owing to degradation caused by atomic

rearrangement or redox chemistry between migrated ions and other species. Evidence suggests that the halides are the most mobile ions in halide perovskites[48, 49]. The activation energy of ion migration has been reported to increase with compressive strain and decrease with tensile strain (Fig. 3d)[16]. This result is consistent with other reports of temperature-dependent conductivity measurements, where increasing compressive strain (relieving tensile strain) results in more stable films[17]. However, here substrates were generally bent along only one axis and so the stress applied was uniaxial. Due to Poisson's effect, there will be strains of opposite signs in the directions perpendicular to the direction of the uniaxial strain. As such, both tensile and compressive strains are expected to exist along different directions in the plane of the film. Furthermore, consideration of the impact of cracks and wrinkles in the film will be needed, as these features may be induced in such bending studies and will affect ion migration. The increasing compressive strain has also been shown to increase the radiation hardness of $CsPbBr_3$ microcrystals (Fig. 3e)[5]. Further, it has been reported that increasing hydrostatic pressure increases the range of miscible I:Br ratios in $MAPb(I_{1-x}Br_x)_3$, and inhibits ion-migration-driven halide segregation[50]. There is still much to be understood about the fundamental mechanisms of halide segregation. Future work will need to explore, for example, how the material's elastic energy changes to maintain the coherency of the underlying lattice in mixed component systems with different ionic sizes[51-53]. The variation of the free energy as a function of composition in alloyed perovskite systems due to coherency strains may, in turn, dictate the miscibility gap of the mixed ions, and elucidate the specific segregation mechanisms[54].

Strain also affects the stability of halide perovskites by regulating the thermodynamics of defect generation. Density functional theory (DFT) calculations show that the defect formation energy of the halide vacancies in halide perovskites decreases with increasing tensile strain[16]. The defect concentration in tensile strained $(FAPbI_3)_{0.85}(MAPbBr_3)_{0.15}$ is reported to be higher than that in its less strained counterpart (2.6×10^{16} versus 2.1×10^{16} cm^{-3})[55]. Moreover, calculations show that shallow defect states in $MAPbI_3$ close to the valence band become even shallower under low hydrostatic pressure (0.3 GPa)[56]. However, in $FAPbI_3$ and $FA_{0.75}Cs_{0.25}PbI_3$, a higher pressure (2 GPa)[45] has been reported to transform shallow iodide vacancy defects into deep level states. More critical comparisons on identical perovskite systems will be needed to generalize such observations. Other computational work suggests that under biaxial strain (compressive or tensile), the lowest energy phase of $MAPbI_3$ is orthorhombic, indicating the presence of a thermodynamic driving force for a phase transition from the desired cubic phase[57]. This contrasts with work on the FA-based analogue showing that compressive strain suppresses the transition from the cubic to tetragonal phase[4]. This is another example of nominally similar halide perovskite systems responding to strain in opposing ways. Similar phase retention behaviour is observed in $MAPbI_3$ films where the tetragonal to orthorhombic phase transition is suppressed for smaller grains[58, 59] which are speculated to be more strained than larger grains, but such strain fields are yet to be directly characterised.

Halide perovskites must also be mechanically robust for photovoltaic applications. Grain boundaries and film edges are sites of abrupt changes in film morphology and structure, and therefore, are regions where stress may be concentrated[60]. Upon loading, a mechanical fracture

can propagate along these boundaries and edges when stress overwhelms the energetic threshold of film fracture. For a given stress value and film thickness, the propensity to crack and delaminate can be calculated through their respective strain energy release rates, G, which scales according to $G \propto \frac{\sigma^2 h}{E}$, where σ is the stress, E is the Young's modulus, and h is the layer thickness[60]. If G exceeds the cohesive fracture energy, Γ_0, (an index reflecting the resistance to mechanical fracture), film cracking and/or delamination will occur. Γ_0 for halide perovskites falls below 1.5 J/m^2, making these materials mechanically vulnerable to fracture[61]. Furthermore, film cracking is more energetically favourable than film delamination (Fig. 3f)[11]. An aim of the field should be to obtain absorber layers with higher Γ_0 (>10 J/m^2)[61] to improve mechanical robustness, with this being even more pertinent for flexible devices[62]. Any residual stresses in perovskites, or adjacent device layers, require careful consideration to minimise the potential of fracturing.

4. Strain engineering to mitigate adverse effects

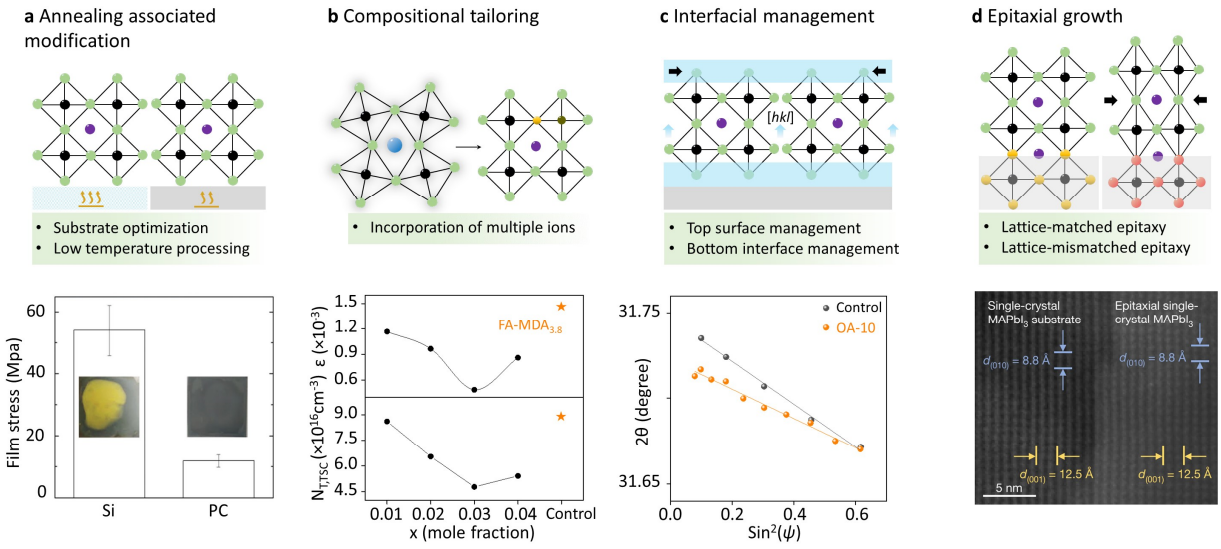

Fig. 4| Strain engineering in halide perovskite photovoltaics. **a**, Annealing associated modification: Top, diagram of how to prevent annealing associated strain generation. Bottom, measured stress for $MAPbI_3$ formed on silicon (Si) and polycarbonate (PC) at 100 °C. Insets show photographs of perovskites deposited on both substrates after 45 h of dry heat aging (85 °C and 25% relative humidity). The perovskite degrades to the yellow phase only on the Si substrate where there is greater thermal expansion mismatch. **b**, Compositional tailoring: Top, illustration of the incorporation of multiple ions. Bottom, microstrain calculated in samples consisting of fluorine-doped tin oxide (FTO)/mesoporous TiO_2/$(FAPbI_3)_{1-x}(MC)_x$ (upper plot) and trap density (lower plot) where MC is a mixture of MDA^{2+} and Cs^+ with the equimolar amount and the orange star indicates control perovskite $[(FAPbI_3)_{0.972}(MDACl_2)_{0.038}]$, $N_{T,\,TSC}$ is the trap density. **c**, Interfacial management: Top, illustration of perovskite interface management. Bottom, linear fit of 2θ vs. $\sin^2\psi$ for n-octylamonium modified (OA-10) and control perovskite films. A reduced slope represents a reduction of tensile stress in perovskite

films. **d**, Epitaxial growth: Top, illustration of epitaxial growth. Bottom, a high-resolution transmission electron microscope image showing the interfacial area of the epitaxial single-crystal $MAPbI_3$ on a $MAPbI_3$ substrate. Figures adapted with permission from: **a**, ref.[20], Wiley-VCH (bottom); **b**, ref.[1], AAAS (bottom); **c**, ref.[55], Wiley-VCH (bottom); **d**, ref.[76], Springer Nature Ltd (bottom).

4.1 Annealing associated modification

Thermal annealing is a routine step in the preparation of polycrystalline perovskites. However, any thermal expansion mismatch between the perovskite thin film and adjacent layers must be considered for strain generation in perovskites and ideally minimised. The bottom panel in Fig. 4a shows aged $MAPbI_3$ films, one on a Si substrate that has degraded to a yellow colour (PbI_2), and the other on a polycarbonate substrate that remains as a dark absorbing film. The difference is attributed to the larger in-plane tensile strain in the film on Si due to the greater CTE mismatch between the perovskite and Si substrate[20]. One way to address this issue is through modification of the annealing process. A variation on standard film fabrication procedures is where the perovskite film is fully formed on the substrate at room temperature (with or without post-annealing) thereby lowering the tensile strain in the film[20]. Another low-temperature approach has enabled photovoltaic devices to deliver an impressive PCE of 23.1% by utilising amine assisted crystallization at room temperature[63]. While these reports show the potential for annealing associated modification of the deposition process, further innovation is required to avoid large residual strains in films. Comparing solution-processed films with thermally evaporated ones (in which the photoactive black perovskite phase can form even without annealing[64]) may also provide insights into any hidden role played by solvent molecules[65]. Further, a vertical temperature gradient through the device stack is present during annealing which can set up chemical and strain gradients along this direction[41]. However, such features are difficult to characterise without depth-dependent and multi-dimensional techniques.

4.2 Compositional tailoring

Compositional tailoring (Fig. 4b) involves substituting different ions into lattice sites and has been reported to be effective in reducing microstrain in halide perovskites. For example, the incorporation of ions with radii smaller than FA (253 pm)[66], such as MA (217 pm)[66] and Cs (167 pm)[66] at the A-site[2, 22], and/or Br (196 pm)[2] and Cl (181 pm)[2] at the X-site[2, 22], has been proposed to reduce the microstrain in $FAPbI_3$-based systems, with a potential strain relaxation mechanism where these additives could decrease the B-X bond lengths and the B-X-B bond angles[2], a conclusion ascertained from DFT calculations[2]. Another approach is to incorporate larger cations (such as PEA) to form 2D or 2D/3D perovskites. This has been shown to promote preferred crystal orientation, reduce Bragg peak width, and increase Bragg peak area (generally indicative of reduced microstrain), yielding improved device efficiency over the 3D-only controls[67]. Recently, simultaneous incorporation of smaller Cs and larger MDA (methylenediammonium; 262 pm) A-site cations into $FAPbI_3$ has been shown to suppress microstrain without increasing the bandgap[1]. The reported microstrain relaxation was associated with a decrease in defect concentration (Fig. 4b, bottom) and nonradiative recombination losses, leading to a PCE of ~24.4% and promising stability[1]. In this work, the

authors note that the simultaneous introduction of larger and smaller ions could modify the local strain in the perovskite lattice, yet the octahedral tilting they proposed, as a mechanism for such microstrain reduction still requires direct experimental evidence. Determination of local atomic structure, for example with pair distribution function analysis, high-resolution electron diffraction, or X-ray fine structure measurements, will be of great value to confirm or refute proposed strain relaxation mechanisms.

Compositional tailoring has achieved success in enhancing device performance but commonly used compositions employing multiple A-site cations (FA/MA or Cs/FA/MA) can be detrimental to the mechanical stability of films[68]. We note that current ubiquitous spin coating procedures including antisolvent quenching can result in smaller grain sizes, which is correlated with a greater susceptibility to film fracture[68], accompanied by reduced cohesive fracture energy, Γ_0. The common practice of using a slight excess of PbI_2 in precursor solutions to achieve higher performances[69] can also reduce film stability[68], in addition to any photo-instabilities it introduces[69]. By contrast, additive species such as 1,2-diaminopropane and butylphosphonic acid 4-ammonium chloride can be added to precursor solutions to crosslink between perovskite grains[61, 70], thereby reducing the film's propensity to mechanically fracture.

4.3 Interfacial management

It is of interest to examine if strain can be modified by inserting an interlayer between the perovskite and the substrate. To date, some compliant interlayers have been reported to relax strain in perovskites caused by CTE mismatch between substrate and perovskite[40, 71]. However, given the thickness of typical interlayers (roughly a few tens of nanometers), the underlying mechanisms are likely to be more complex. For example, the use of a compliant polytriarylamine interlayer on top of a Si substrate, with a thickness of ~20 nm, will not have a significant effect on alleviating the CTE-mismatch-induced strain experienced by the top perovskite layers[20]. Furthermore, despite claims in recent reports[18, 72], interlayers are unlikely to facilitate strain control by minimising the lattice mismatch at the interface because the perovskite growth processes are unlikely to be epitaxial[73] (owing to the typical solution processing methods of these films) and thus lattice matching with the substrate may, in general, not be relevant. In other work, it has been proposed that the top contact layer can be modified for use as a strain compensation layer. For example, poly[5,5-bis(2-butyloctyl)-(2,2-bithiophene)-4,4′-dicarboxylate-alt-5,5′-2,2′-bithiophene], which has a larger CTE than $CsPbI_2Br$, could lead to a compressive strain on the $CsPbI_2Br$ layer below, offsetting the residual tensile strain in the perovskite[16]. Constructing a 2D perovskite layer on top of the 3D perovskite has also been shown to reduce the residual stress in perovskites (Fig. 4c, bottom)[55], based on 2D perovskites exhibiting a lower Young's modulus. However, care must be taken to determine whether the corresponding stress and strain reductions in perovskites are truly due to the mechanical action of these contact layers. Furthermore, efforts should be made to assess the stress and strain evolution at the 2D/3D interface, which is likely to be influenced by the orientation of the 2D perovskites relative to their 3D counterpart[74]. Besides, not all 2D/3D interfaces will be sufficiently stable without further management: for instance, it has been

proposed that invasive ions from the underlying 3D perovskites interrupt the Van der Waals interactions in the 2D layered perovskites[75], which could drive layer slippage and even fracture.

Epitaxy is a well-established material growth technique for introducing controlled levels of strain into materials by judiciously choosing lattice-matched/mismatched substrates. Recently, successful epitaxial growth of α-$FAPbI_3$ was achieved by tailoring the composition of a $MAPbCl_xBr_{3-x}$ single-crystal substrate[4]. Further compositional tuning also allowed various levels of strain to be imparted onto the α-$FAPbI_3$ epilayer, with low levels of compressive strain found to notably enhance the phase stability. In other work, solution-phase epitaxial growth of $MAPbI_3$ was enabled by using lattice-matched $MAPbI_3$ substrates (Fig. 4d, bottom), with an impressively large area (>25 cm^2) and the absence of dislocations[76]. Heteroepitaxial growth of halide perovskites directly on top of charge transport layers could be useful, but this will further necessitate expanding the current library of contact layers for halide perovskite devices. Another interesting aspect of epitaxial growth is the tendency of phase impurities to epitaxially grow alongside perovskite phases[77]. Given the critical need to minimise phase impurities, especially those harmful to performance and stability, further research is needed to understand the role of epitaxial growth in stabilising halide perovskites. Nonetheless, epitaxial techniques are comparatively expensive and their use risks negating this key advantage of halide perovskites (that of inexpensive and scalable processability) in the face of more efficient and stable III-V or Si-based equivalents.

In addition, it has been reported that some contact layers in perovskite photovoltaics suffer intrinsic fragility[78] or inadequate adhesion to the perovskites[79-81], and perovskite photovoltaics with these undesirable characteristics will have reduced stress tolerance and mechanical integrity. Approaches to address this issue have been proposed, including the design of materials in which strong covalent bonds can form after deposition from the solution state[78], the use of self-assembled interlayers[79], low-dimensional perovskite capping layers on top of 3D perovskites[80], and graded interfaces[81]. Such approaches will be critical for increasing the film's cohesive fracture energy, Γ_0, and ensuring mechanical integrity of the operating devices[79].

5. Challenges and Outlook

To tackle the many outstanding questions about the links between strain and material properties in perovskite photovoltaics, we propose an iterative workflow whereby strain is tuned with advanced strain engineering (Fig. 5a), and more fully characterised using powerful in situ and ex situ measurement techniques (Fig. 5b) with the knowledge fed back to improve strain engineering approaches. Finally, the result (Fig. 5c) will be the ability to not only suppress the adverse effects of strain but also to exploit strain for favourable outcomes in devices.

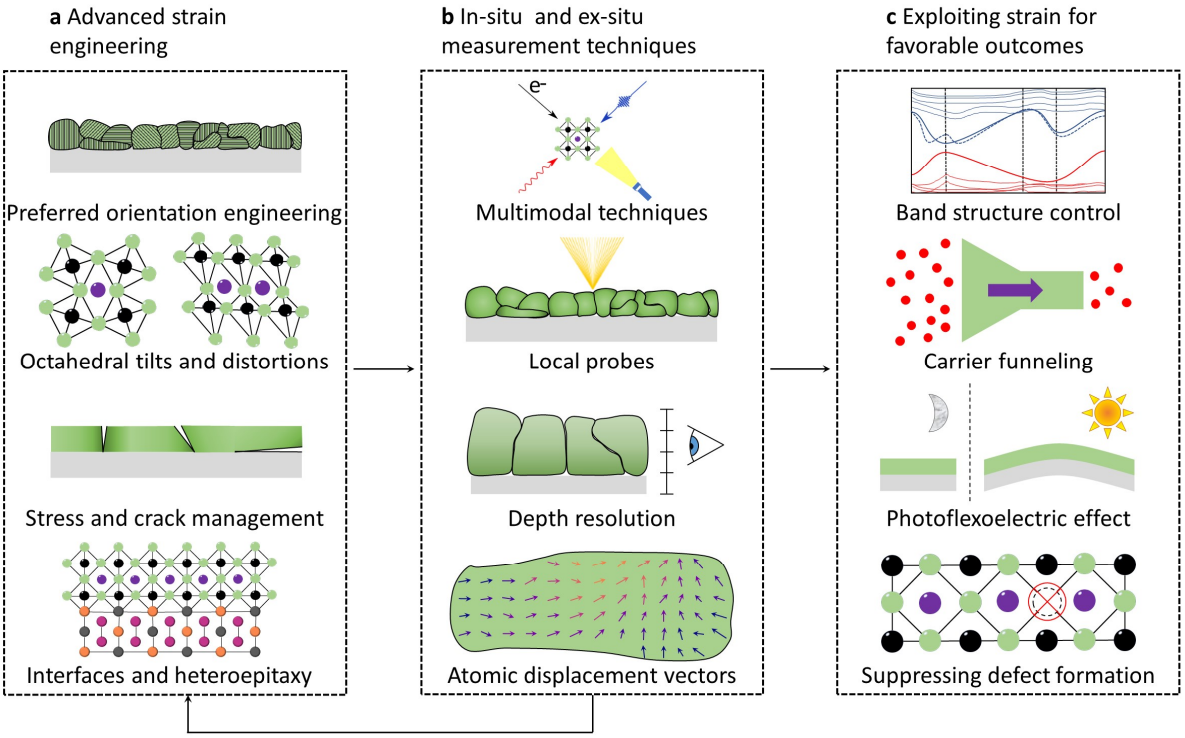

Fig. 5| Workflow for unlocking the potential of strain in perovskite devices. a, Strain can be applied systematically to halide perovskites with advanced strain engineering. **b**, Cutting-edge in- and ex-situ characterisation techniques are employed to fully characterise strain in halide perovskite samples. **c**, Strain is exploited to realise better devices.

5. 1 Advanced strain engineering

The association of nonradiative losses with orientation mismatch[36] suggests that engineering films with greater preferred orientation should be targeted for improved optoelectronic properties. Further, one may be able to channel strain into crystallographic directions where the presence of strain is less detrimental. For example, microstrain in $FAPbI_3$ in the ⟨111⟩ direction, in particular, is associated with reduced film stability[22]. Meanwhile, Young's modulus exhibits a directional anisotropy, with $E_{110} < E_{100}$, in cubic $MAPbX_3$ (X=Br, Cl), making it more facile for deformations to propagate in the ⟨110⟩ direction than in the ⟨100⟩ direction[82]. However, care must be taken when extracting microstrain values for particular crystallographic directions from individual Bragg peaks, especially if assuming negligible crystallite size broadening based on the morphological grain size given the presence of sub-grain heterogeneities[13].

Tilting of the octahedral BX_6^{4-} units has been well studied in other systems based on the perovskite structure[83] and octahedral distortions including cation off-centring are also known in halide perovskites. However, study of octahedral tilting and distortion in halide perovskites are often limited to Goldschmidt tolerance factor considerations, which leads to difficulties when considering molecular cations that can form hydrogen bonds[83]. Although some researchers have noted the link between octahedral tilting/distortion and strain[84], explicit

characterisations of such structural features will be critical given the relationship between important properties such as bandgap and the largest metal-halide-metal bond angle[85].

The determination of stress and its impact on halide perovskites are under-explored areas and merit more dedicated studies. Uncompensated stress can cause fracturing of the perovskite leading to the loss of Ohmic contacts with the charge-selective layers and allowing the ingress of detrimental moisture and oxygen[86]. Stress analyses could explain film wrinkling, a common mechanism by which a film can relieve stress during formation[87]. Additionally, from a thermodynamic perspective, spatially heterogeneous distributions of stress can result in the local accumulation of elastic energy in films which is relevant given ions will rearrange until their diffusion potentials are uniform across the film[51]. Stresses will occur on both short and long length scales, with delamination[60] and cracking[88] being problems at the scale of tens of micrometres, and emergent microstresses at the grain boundaries and other operational stresses being concerns on the nano to atomic scale[11, 89]. Defect pooling at grain interfaces can reduce the material's mechanical integrity by causing these interfaces to serve as fracture points[61]. Given the presence of sub-grain features and misorientations, solving the above issues will likely require strategies beyond just tuning processing methods. Stress can either be determined directly through curvature measurements[20, 35, 87], or calculated indirectly, via interrogation of strain ascertained through material structure studies with use of appropriate proportionality constants. However, such indirect calculations of stress come with many complexities[88, 90]. A common method for the measurement of the in-plane residual stresses in films is the $\sin^2\psi$ method[88, 90].

Beyond the perovskite bulk, regulating harmful strain at the substrate/perovskite interface is also crucial for improving device performance. Substrates with aligned nanopores have been employed to confine crystallization and impose compressive strain on perovskites, with the strain level dependent on the pore size[91]. Similar results are achieved through the manufacture of textured perovskite films[92]. Furthermore, perovskites that are infiltrated into a porous TiO_2/ZrO_2/Carbon layer have been shown to exhibit improved mechanical integrity[68]. Another emerging approach to reduce strain is to apply 2D materials (such as transition metal dichalcogenides) as interlayers where the Van der Waals interaction enables perovskites to expand/contract freely during heating/cooling processes[93]. We note, however, the key challenge of synthesising such 2D materials without dangling bonds. Regulating strain may also involve management of lattice matching at semiconductor interfaces, but this approach has received limited attention to date, probably for two reasons: first, there is a debate about whether typical solution processing of perovskites involves epitaxial growth processes, and second, the perovskite structure is sufficiently accommodating that device efficiencies have not suffered appreciably in the face of poorly lattice-matched interfaces. However, it is possible that some more sinister ramifications of poor lattice matching, such as delamination of layers in the device stack, only become evident after stringent, long-term operational testing[61]. Looking towards conventional semiconductors, epitaxial growth of perovskites on hetero-substrates can allow control of strain at the interface by tuning lattice matching. A halide perovskite epilayer grown on functional layers, without secondary transfer of the epitaxial perovskite, could be desirable for high-performance photovoltaic applications, and there is a

wealth of literature on other materials with domain matching epitaxy[94]. Additionally, the application of intervening layers allows high-quality epitaxial growth of semiconductors with strain applied through carefully chosen lattice mismatches[60].

The strain management methods proposed in this work will apply to a wide range of perovskite-based photovoltaics including Sn- and Sn-Pb based devices[95, 96] and tandem cells[97]. Effective strain management will also be critical when employing perovskites on flexible substrates or upscaling to full-sized modules[68]. Additionally, daily or seasonal temperature, spectral, and light intensity changes present important challenges for both stress and strain management in operating devices.

5.2 In and ex situ measurement techniques

Multimodal correlative microscopy can provide deep insights into the underlying physics in halide perovskites. For example, correlation of strain fields with photoluminescence, compositional, and time-resolved data sets will uncover new links between strain and material performance[3, 36]. Integrating tight environmental control (of light, heat, humidity, UV exposure, etc.) and sample encapsulation with these measurement techniques will allow assessment of the evolution of strain in operating devices.

The presence of spatially heterogeneous strain in halide perovskite samples necessitates the use of local probes for studying strain. Current state-of-the-art film compositions contain many components which are known to segregate[98, 99]. To adequately assess the impacts of this segregation, a local approach to strain characterisation is required, further employing techniques such as scanning probe nano-XRD and X-ray fluorescence[100]. There is also evidence for rich chemical heterogeneity at the grain and sub-grain length scales[13].

In alloyed systems[66], including the Pb/Sn and mixed cation and halide systems, it is still unclear how the alloyed components are arranged – whether they vary from unit cell to unit cell, or if they tend to form clusters across the sample[101]. In the case of mixed halide samples, given the evidence for inhomogeneous halide distributions[42], the observed compressive/tensile "strain" may be due to changes in composition rather than stress. The community, therefore, needs to expand its understanding of local chemical distributions through the use of nanoscale chemical mapping techniques[102, 103]. Further, ion re-distribution in perovskites can gradually occur in response to strain, which, in turn, varies the strain distribution in perovskites[16]. To overcome these challenges, in-situ strain detection is required to view strain propagation in real-time.

Strain measurements to date have predominantly focused on the in-plane direction, and further work to simultaneously monitor out-of-plane strain is of interest. Furthermore, the relative importance of strain in the perovskite bulk and strain at the perovskite surface is currently unknown. A greater focus on depth-resolved techniques such as grazing incidence X-ray scattering will be required.

Most reports on strain to date have been on neat film samples as opposed to device stacks, and so these works miss the complex interactions of the perovskite with adjacent layers in the

device. Local heterogeneities in the perovskite material may also exist due to the influence of other device layers. Under electrical bias, there is evidence for photostrictive effects along with ion migration[48], the activation energy of which can be altered by strain and is a vitally important phenomenon to understand in the field. Thus, developing techniques for in operando characterisations of microstrain in full and half devices for a complete understanding of the impact of strain will be fruitful.

Advanced coherent diffraction imaging techniques such as Bragg coherent diffraction imaging and Bragg ptychography can potentially allow reconstruction of full three-dimensional maps of atomic displacement vectors[104]. Resolving atomic displacement vectors would allow one to uncover strain fields in halide perovskites that may be characteristic of certain crystal aberrations, facilitating "defect diagnosis"[14]. Correlation of these strain fields with other optoelectronic data would yield rich insights and should be a future research focus. Atomic displacement vectors can also be resolved with cryogenic and high-resolution transmission electron microscopy measurements [77, 105]. However, attention must be paid to the beam dose in these measurements, which might introduce undesirable defects and/or lead to material decomposition if not performed carefully[106, 107].

5.3 Exploiting strain for favourable outcomes

There is a wealth of literature on using strain in other material systems to enhance material characteristics by modulating band structures[108], electrical conductivities[109], electron-phonon coupling and ion migration[110], among other properties[111]. Modulating strain could see several exotic effects realised in halide perovskites leading to new device use-cases. First-principles computational work suggests polar phases in lead-iodide perovskites may be realisable with large Rashba splitting at room temperature via tensile strain[112]. Being able to control Rashba splitting provides an additional lever for tuning carrier dynamics[113]. Distinct chemical domains with distinct bandgaps within mixed-component films may allow for carrier funnelling and devices based on such effects[3,41,114]. Strain gradients have also been utilised in halide perovskites to enhance flexoelectric responses with corresponding photoflexoelectric effects demonstrated in $MAPbI_3$ single crystals[115]. While engineering such exotic effects into real-world devices is yet to be realised, these reports show that strain plays a critical role in the electronic structure of halide perovskites, and that it can indeed be exploited. Strain management can lead to better material quality by suppressing the formation of defects due to ion migration in the material.

A robust understanding of the origins and effects of strain in halide perovskite-based devices is needed to facilitate future breakthroughs. This will be especially critical in the construction of perovskite/Si and perovskite/perovskite tandems, where many layers may each contribute both stress and strain components, influencing overall efficiency and stability. As the halide perovskite community continues to push the envelope on long-term operational stability, strain will be a key parameter for optimisation and a versatile lever for control in more exotic devices.

Acknowledgements

W.Z. acknowledges UK Engineering and Physical Sciences Research Council (EPSRC) New Investigator Award (2018; EP/R043272/1) and Newton Advanced Fellowship (192097) for financial support. S.D.S. acknowledges the support from Royal Society and Tata Group (UF150033), the European Research Council (ERC) under the European Union's Horizon 2020 research and innovation programme (HYPERION, grant agreement No. 756962) and EPSRC under grant reference EP/R023980/1. D.L.(Liu) acknowledges China Scholarship Council (CSC, No. 201908310074) for financial support. D.L. and Z.-H.L. acknowledge the Natural Science and Engineering Research Council of Canada. A.N.I. acknowledges a scholarship from the British Spanish Society. K.W.P.O. acknowledges funding from an EPSRC studentship. T.A.S.D. acknowledges support of a National University of Ireland (NUI) Travelling Studentship. The authors acknowledge Dr Miguel Anaya for fruitful discussions.

Author contributions

D. Liu, D. Luo., A.N.I. and K.W.P.O. contributed equally to conceiving and writing the first draft. All authors contributed to the discussion of content and revisions of the manuscript.

Competing interests

S.D.S. is a co-founder of Swift Solar, Inc. All other authors declare no competing interest.

Additional information

Correspondence should be addressed to W.Z. and S.D.S.

References

1. Kim, G. et al. Impact of strain relaxation on performance of α-formamidinium lead iodide perovskite solar cells. *Science* **370**, 108-112 (2020).
2. Saidaminov, M.I. et al. Suppression of atomic vacancies via incorporation of isovalent small ions to increase the stability of halide perovskite solar cells in ambient air. *Nat. Energy* **3**, 648-654 (2018).
3. Jones, T.W. et al. Lattice strain causes non-radiative losses in halide perovskites. *Energy Environ. Sci.* **12**, 596-606 (2019).
4. Chen, Y. et al. Strain engineering and epitaxial stabilization of halide perovskites. *Nature* **577**, 209-215 (2020).
5. Li, X., Luo, Y., Holt, M.V., Cai, Z. & Fenning, D.P. Residual nanoscale strain in cesium lead bromide perovskite reduces stability and shifts local luminescence. *Chem. Mater.* **31**, 2778-2785 (2019).
6. Chen, A., Yossef, M. & Zhang, C. Strain effect on the performance of amorphous silicon and perovskite solar cells. *Sol. Energy* **163**, 243-250 (2018).
7. Yang, C., Song, K., Xu, X., Yao, G. & Wu, Z. Strain dependent effect on power degradation of CIGS thin film solar cell. *Sol. Energy* **195**, 121-128 (2020).
8. Watson, B.L., Rolston, N., Printz, A.D. & Dauskardt, R.H. Scaffold-reinforced perovskite compound solar cells. *Energy Environ. Sci.* **10**, 2500-2508 (2017).
9. Yang, B. Stress, strain, and structural dynamics. (Elsevier Acadmic Press, 2005).

10. Sun, Y., Thompson, S.E. & Nishida, T. Strain effect in semiconductors: theory and device applications. (Springer Science & Business Media, 2009).
11. Ramirez, C., Yadavalli, S.K., Garces, H.F., Zhou, Y. & Padture, N.P. Thermo-mechanical behavior of organic-inorganic halide perovskites for solar cells. *Scr. Mater.* **150**, 36-41 (2018).
12. Pecharsky, V. & Zavalij, P. Fundamentals of powder diffraction and structural characterization of materials. (Springer Science & Business Media, 2008).
13. Tennyson, E.M., Doherty, T.A.S. & Stranks, S.D. Heterogeneity at multiple length scales in halide perovskite semiconductors. *Nat. Rev. Mater.* **4**, 573-587 (2019).
14. Robinson, I. & Harder, R. Coherent X-ray diffraction imaging of strain at the nanoscale. *Nat. Mater.* **8**, 291-298 (2009).
15. Rodenburg, J.M. Ptychography and related diffractive imaging methods. *Adv. Imaging Electron Phys*. **150**, 87-184 (2008).
16. Xue, D.J. et al. Regulating strain in perovskite thin films through charge-transport layers. *Nat. Commun.* **11**, 1514 (2020).
17. Zhao, J. et al. Strained hybrid perovskite thin films and their impact on the intrinsic stability of perovskite solar cells. *Sci. Adv.* **3**, eaao5616 (2017).
18. Zhang, B. et al. NiO/perovskite heterojunction contact engineering for highly efficient and stable perovskite solar cells. *Adv. Sci.* **7**, 1903044 (2020).
19. Zhang, C.C. et al. Perovskite films with reduced interfacial strains via a molecular-level flexible interlayer for photovoltaic application. *Adv. Mater.* **32**, e2001479 (2020).
20. Rolston, N. et al. Engineering stress in perovskite solar cells to improve stability. *Adv. Energy Mater.* **8**, 1802139 (2018).
21. Jiao, Y. et al. Strain engineering of metal halide perovskites on coupling anisotropic behaviors. *Adv. Funct. Mater.* **31**, 2006243 (2021).
22. Zheng, X. et al. Improved phase stability of formamidinium lead triiodide perovskite by strain relaxation. *ACS Energy Lett.* **1**, 1014-1020 (2016).
23. Howard, C.J. & Stokes, H.T. Group-theoretical analysis of octahedral tilting in perovskites. *Acta Cryst. B* **54**, 782-789 (1998).
24. Carpenter, M.A. et al. Structural evolution, strain and elasticity of perovskites at high pressures and temperatures. *J. Mineral. Petrol. Sci.* **101**, 95-109 (2006).
25. Carpenter, M.A., Becerro, A.I. & Seifert, F. Strain analysis of phase transitions in (Ca,Sr)TiO_3 perovskites. *Am. Mineral.* **86**, 348-363 (2001).
26. Khachaturyan, A.G. Theory of structural transformations in solids. (Courier Corporation, 2013).
27. Chou, C.C. & Wayman, C.M. Cubic to tetragonal martensitic transformation in lead titanate ($PbTiO_3$) single crystals. *Mater. Trans. JIM* **33**, 306-317 (1992).
28. Bhadeshia, H.K.D.H. Martensite in Steels. *Department of Materials Science & Metallurgy, University of Cambridge* (2020).
29. Prakash, A. et al. Self-assembled periodic nanostructures using martensitic phase transformations. *Nano Lett.* **21**, 1246-1252 (2021).
30. Kim, D. et al. Light- and bias-induced structural variations in metal halide perovskites. *Nat. Commun.* **10**, 444 (2019).

31. Brennan, M.C., Draguta, S., Kamat, P.V. & Kuno, M. Light-induced anion phase segregation in mixed halide perovskites. *ACS Energy Lett.* **3**, 204-213 (2018).
32. Bischak, C.G. et al. Origin of reversible photoinduced phase separation in hybrid perovskites. *Nano Lett.* **17**, 1028-1033 (2017).
33. Muscarella, L.A. et al. Lattice compression increases the activation barrier for phase segregation in mixed-halide perovskites. *ACS Energy Lett.* **5**, 3152-3158 (2020).
34. Tsai, H. et al. Light-induced lattice expansion leads to high-efficiency perovskite solar cells. *Science* **360**, 67-70 (2018).
35. Rolston, N. et al. Comment on "Light-induced lattice expansion leads to high-efficiency perovskite solar cells". *Science* **368**, eaay8691 (2020).
36. Jariwala, S. et al. Local crystal misorientation influences non-radiative recombination in halide perovskites. *Joule* **3**, 3048-3060 (2019).
37. Doherty, T.A.S. et al. Performance-limiting nanoscale trap clusters at grain junctions in halide perovskites. *Nature* **580**, 360-366 (2020).
38. Hytch, M.J., Putaux, J.L. & Thibault, J. Stress and strain around grain-boundary dislocations measured by high-resolution electron microscopy. *Philos. Mag.* **86**, 4641-4656 (2006).
39. Xiao, X. et al. Benign ferroelastic twin boundaries in halide perovskites for charge carrier transport and recombination. *Nat. Commun.* **11**, 2215 (2020).
40. Yang, W., Zhong, D., Shi, M., Qu, S. & Chen, H. Toward highly thermal stable perovskite solar cells by rational design of interfacial layer. *iScience* **22**, 534-543 (2019).
41. Zhu, C. et al. Strain engineering in perovskite solar cells and its impacts on carrier dynamics. *Nat. Commun.* **10**, 815 (2019).
42. Feldmann, S. et al. Photodoping through local charge carrier accumulation in alloyed hybrid perovskites for highly efficient luminescence. *Nat. Photonics* **14**, 123-128 (2020).
43. Prasanna, R. et al. Band gap tuning via lattice contraction and octahedral tilting in perovskite materials for photovoltaics. *J. Am. Chem. Soc.* **139**, 11117-11124 (2017).
44. McKenna, K.P. Electronic properties of {111} twin boundaries in a mixed-ion lead halide perovskite solar absorber. *ACS Energy Lett.* **3**, 2663-2668 (2018).
45. Ghosh, D., Aziz, A., Dawson, J.A., Walker, A.B. & Islam, M.S. Putting the squeeze on lead iodide perovskites: pressure-induced effects to tune their structural and optoelectronic behavior. *Chem. Mater.* **31**, 4063-4071 (2019).
46. Du, Q. et al. Stacking effects on electron–phonon coupling in layered hybrid perovskites via microstrain manipulation. *ACS Nano* **14**, 5806-5817 (2020).
47. Dou, L. et al. Atomically thin two-dimensional organic-inorganic hybrid perovskites. *Science* **349**, 1518-1521 (2015).
48. Walsh, A. & Stranks, S.D. Taking control of ion transport in halide perovskite solar cells. *ACS Energy Lett.* **3**, 1983-1990 (2018).
49. Yang, T.Y., Gregori, G., Pellet, N., Gratzel, M. & Maier, J. The significance of ion conduction in a hybrid organic-inorganic lead-iodide-based perovskite photosensitizer. *Angew. Chem. Int. Ed.* **54**, 7905-7910 (2015).
50. Hutter, E.M. et al. Thermodynamic stabilization of mixed-halide perovskites against phase segregation. *Cell Rep. Phys. Sci.* **1**, 100120 (2020).

720 51. Voorhees, P.W. & Johnson, W.C. The thermodynamics of elastically stressed crystals.
721 *Solid State Phys.* **59**, 1-201 (2004).
722 52. Cahn, J.W. Coherent fluctuations and nucleation in isotropic solids. *Acta Metall.* **10**,
723 907-913 (1962).
724 53. Cook, H.E. & de Fontaine, D. On the elastic free energy of solid solutions—I.
725 Microscopic theory. *Acta Metall.* **17**, 915-924 (1969).
726 54. Heimann, R.B. *Classic and advanced ceramics: from fundamentals to applications*.
727 (Wiley-VCH, 2010).
728 55. Wang, H. et al. Interfacial residual stress relaxation in perovskite solar cells with
729 improved stability. *Adv. Mater.* **31**, 1904408 (2019).
730 56. Kong, L. et al. Simultaneous band-gap narrowing and carrier-lifetime prolongation of
731 organic-inorganic trihalide perovskites. *Proc. Natl. Acad. Sci. U. S. A.* **113**, 8910-8915
732 (2016).
733 57. Ong, K.P., Goh, T.W., Xu, Q. & Huan, A. Structural evolution in methylammonium
734 lead iodide $CH_3NH_3PbI_3$. *J. Mater. Chem. A* **119**, 11033-11038 (2015).
735 58. Osherov, A. et al. The impact of phase retention on the structural and optoelectronic
736 properties of metal halide perovskites. *Adv. Mater.* **28**, 10757-10763 (2016).
737 59. Stavrakas, C. et al. Influence of grain size on phase transitions in halide perovskite films.
738 *Adv. Energy Mater.* **9**, 1901883 (2019).
739 60. Freund, L.B. & Suresh, S. *Thin film materials: stress, defect formation and surface*
740 *evolution*. (Cambridge University Press, Cambridge; 2004).
741 61. Rolston, N. et al. Mechanical integrity of solution-processed perovskite solar cells.
742 *Extreme Mech. Lett.* **9**, 353-358 (2016).
743 62. Chen, H. et al. Flexible optoelectronic devices based on metal halide perovskites. *Nano*
744 *Res.* **13**, 1997-2018 (2020).
745 63. Wang, K. et al. Isothermally crystallized perovskites at room-temperature. *Energy*
746 *Environ. Sci.* **13**, 3412-3422 (2020).
747 64. Dewi, H.A. et al. Excellent intrinsic long-term thermal stability of co-evaporated
748 $MAPbI_3$ solar cells at 85 °C. *Adv. Funct. Mater.* **31**, 2100557 (2021).
749 65. Chiang, Y.-H., Anaya, M. & Stranks, S.D. Multisource vacuum deposition of
750 methylammonium-free perovskite solar cells. *ACS Energy Lett.* **5**, 2498-2504 (2020).
751 66. Saliba, M. et al. Incorporation of rubidium cations into perovskite solar cells improves
752 photovoltaic performance. *Science* **354**, 206-209 (2016).
753 67. Lee, J.-W. et al. 2D perovskite stabilized phase-pure formamidinium perovskite solar
754 cells. *Nat. Commun.* **9**, 3021 (2018).
755 68. Rolston, N. et al. Effect of cation composition on the mechanical stability of perovskite
756 solar cells. *Adv. Energy Mater.* **8**, 1702116 (2018).
757 69. Roose, B., Dey, K., Chiang, Y.-H., Friend, R.H. & Stranks, S.D. Critical assessment of
758 the use of excess lead iodide in lead halide perovskite solar cells. *J. Phys. Chem. Lett.*
759 **11**, 6505-6512 (2020).
760 70. Li, X. et al. Improved performance and stability of perovskite solar cells by crystal
761 crosslinking with alkylphosphonic acid ω-ammonium chlorides. *Nat. Chem.* **7**, 703-711
762 (2015).

71. Wu, J. et al. A simple way to simultaneously release the interface stress and realize the inner encapsulation for highly efficient and stable perovskite solar cells. *Adv. Funct. Mater.* **29**, 1905336 (2019).
72. Cao, J. et al. Enhanced performance of planar perovskite solar cells induced by Van Der Waals epitaxial growth of mixed perovskite films on WS_2 flakes. *Adv. Funct. Mater.* **30**, 2002358 (2020).
73. Lu, C. & Tang, L. Comment on "Spin coating epitaxial films". *Science* **365**, eaay3894 (2019).
74. Tu, Q. et al. Out-of-plane mechanical properties of 2D hybrid organic–inorganic perovskites by nanoindentation. *ACS Appl. Mater. Interfaces* **10**, 22167-22173 (2018).
75. Zhang, C. et al. Fabrication strategy for efficient 2D/3D perovskite solar cells enabled by diffusion passivation and strain compensation. *Adv. Energy Mater.* **10**, 2002004 (2020).
76. Lei, Y. et al. A fabrication process for flexible single-crystal perovskite devices. *Nature* **583**, 790-795 (2020).
77. Rothmann, M.U. et al. Atomic-scale microstructure of metal halide perovskite. *Science* **370**, eabb5940 (2020).
78. Watson, B.L. et al. Cross-linkable, solvent-resistant fullerene contacts for robust and efficient perovskite solar cells with increased J_{SC} and V_{OC}. *ACS Appl. Mater. Interfaces* **8**, 25896-25904 (2016).
79. Dai, Z. et al. Interfacial toughening with self-assembled monolayers enhances perovskite solar cell reliability. *Science* **372**, 618-622 (2021).
80. Dong, Q. et al. Flexible perovskite solar cells with simultaneously improved efficiency, operational stability, and mechanical reliability. *Joule* **5**, 1587-1601 (2021).
81. Dong, Q. et al. Interpenetrating interfaces for efficient perovskite solar cells with high operational stability and mechanical robustness. *Nat. Commun.* **12**, 973 (2021).
82. Sun, S., Fang, Y., Kieslich, G., White, T.J. & Cheetham, A.K. Mechanical properties of organic–inorganic halide perovskites, $CH_3NH_3PbX_3$ (X = I, Br and Cl), by nanoindentation. *J. Mater. Chem. A* **3**, 18450-18455 (2015).
83. Glazer, A.M. The classification of tilted octahedra in perovskites. *Acta Cryst. B* **28**, 3384-3392 (1972).
84. Bechtel, J.S. & Van der Ven, A. Octahedral tilting instabilities in inorganic halide perovskites. *Phys. Rev. Mater.* **2**, 025401 (2018).
85. Filip, M.R., Eperon, G.E., Snaith, H.J. & Giustino, F. Steric engineering of metal-halide perovskites with tunable optical band gaps. *Nat. Commun.* **5**, 5757 (2014).
86. Boyd, C.C., Cheacharoen, R., Leijtens, T. & McGehee, M.D. Understanding degradation mechanisms and improving stability of perovskite photovoltaics. *Chem. Rev.* **119**, 3418-3451 (2019).
87. Bush, K.A. et al. Controlling thin-film stress and wrinkling during perovskite film formation. *ACS Energy Lett.* **3**, 1225-1232 (2018).
88. Yadavalli, S.K., Dai, Z., Zhou, H., Zhou, Y. & Padture, N.P. Facile healing of cracks in organic–inorganic halide perovskite thin films. *Acta Mater.* **187**, 112-121 (2020).
89. Dai, Z. et al. Effect of grain size on the fracture behavior of organic-inorganic halide perovskite thin films for solar cells. *Scr. Mater.* **185**, 47-50 (2020).

90. Birkholz, M. *Thin film analysis by X-ray scattering*. (Wiley-VCH, 2006).
91. Ma, S. et al. Strain-mediated phase stabilization: a new strategy for ultrastable α-$CsPbI_3$ perovskite by nanoconfined growth. *Small* **15**, 1900219 (2019).
92. Steele, J.A. et al. Thermal unequilibrium of strained black $CsPbI_3$ thin films. *Science* **365**, 679-684 (2019).
93. Kum, H. et al. Epitaxial growth and layer-transfer techniques for heterogeneous integration of materials for electronic and photonic devices. *Nat. Electron.* **2**, 439-450 (2019).
94. Narayan, J. & Larson, B.C. Domain epitaxy: a unified paradigm for thin film growth. *J. Appl. Phys.* **93**, 278-285 (2002).
95. Nishimura, K. et al. Relationship between lattice strain and efficiency for Sn-perovskite solar cells. *ACS Appl. Mater. Interfaces* **11**, 31105-31110 (2019).
96. Kapil, G. et al. Strain relaxation and light management in tin–lead perovskite solar cells to achieve high efficiencies. *ACS Energy Lett.* **4**, 1991-1998 (2019).
97. Li, H. & Zhang, W. Perovskite tandem solar cells: from fundamentals to commercial deployment. *Chem. Rev.* **120**, 9835-9950 (2020).
98. Knight, A.J. & Herz, L.M. Preventing phase segregation in mixed-halide perovskites: a perspective. *Energy Environ. Sci.* **13**, 2024-2046 (2020).
99. Grüninger, H. et al. Microscopic (dis)order and dynamics of cations in mixed FA/MA lead halide perovskites. *J. Phys. Chem. C* **125**, 1742-1753 (2021).
100. Kodur, M. et al. X-ray microscopy of halide perovskites: techniques, applications, and prospects. *Adv. Energy Mater.* **10**, 1903170 (2020).
101. Wu, C., Chen, K., Guo, D.Y., Wang, S.L. & Li, P.G. Cations substitution tuning phase stability in hybrid perovskite single crystals by strain relaxation. *Rsc Adv.* **8**, 2900-2905 (2018).
102. Szostak, R. et al. Nanoscale mapping of chemical composition in organic-inorganic hybrid perovskite films. *Sci. Adv.* **5**, eaaw6619 (2019).
103. Liu, Y. et al. Chemical nature of ferroelastic twin domains in $CH_3NH_3PbI_3$ perovskite. *Nat. Mater.* **17**, 1013-1019 (2018).
104. Newton, M.C., Leake, S.J., Harder, R. & Robinson, I.K. Three-dimensional imaging of strain in a single ZnO nanorod. *Nat. Mater.* **9**, 120-124 (2010).
105. Li, Y. et al. Unravelling degradation mechanisms and atomic structure of organic-inorganic halide perovskites by cryo-EM. *Joule* **3**, 2854-2866 (2019).
106. Rothmann, M.U., Li, W., Etheridge, J. & Cheng, Y.-B. Microstructural characterisations of perovskite solar cells – from grains to interfaces: techniques, features, and challenges. *Adv. Energy Mater.* **7**, 1700912 (2017).
107. Zhou, Y., Sternlicht, H. & Padture, N.P. Transmission electron microscopy of halide perovskite materials and devices. *Joule* **3**, 641-661 (2019).
108. Hong, K.-H., Kim, J., Lee, S.-H. & Shin, J.K. Strain-driven electronic band structure modulation of Si nanowires. *Nano Lett.* **8**, 1335-1340 (2008).
109. Manzeli, S., Allain, A., Ghadimi, A. & Kis, A. Piezoresistivity and strain-induced band gap tuning in atomically thin MoS_2. *Nano Lett.* **15**, 5330-5335 (2015).
110. Si, C., Sun, Z. & Liu, F. Strain engineering of graphene: a review. *Nanoscale* **8**, 3207-3217 (2016).

111. Jia, M.Z. et al. Exploring ion migration in Li_2MnSiO_4 for Li-ion batteries through strain effects. *Rsc Adv.* **7**, 26089-26096 (2017).
112. Leppert, L., Reyes-Lillo, S.E. & Neaton, J.B. Electric field- and strain-induced Rashba effect in hybrid halide perovskites. *J. Phys. Chem. Lett.* **7**, 3683-3689 (2016).
113. Stranks, S.D. & Plochocka, P. The influence of the Rashba effect. *Nat. Mater.* **17**, 381-382 (2018).
114. Yuan, M. et al. Perovskite energy funnels for efficient light-emitting diodes. *Nat. Nanotechnol.* **11**, 872-877 (2016).
115. Shu, L. et al. Photoflexoelectric effect in halide perovskites. *Nat. Mater.* **19**, 605-609 (2020).